# Exercise 3
# A lid-driven cavity flow

**41319 - Computational Fluid Dynamics**

by

**Thomas Sørensen s113354**

**Franz Hastrup-Nielsen s113399**

**Department of Mechanical Engineering -**
**Fluid Mechanics, Coastal & Maritime Engineering**
**Technical University of Denmark**
**13. November 2015**

# Contents

# 1 Introduction

This report describes the simulation of a translating lid flow in a square cavity. To do this the nondimensional incompressible unsteady 2D Navier-Stokes equations are used. The method used is the finite volume method on a staggered cartesian grid with square uniform cells with the central difference scheme applied.
The advantage of using a staggered grid is an improved accuracy and stability of the algorithm avoiding odd-even decoupling and non-physical solutions while the disadvantage is to keep track of the different grids used.

# 2 Non-dimensionalization of the momentum equation

The dimensional forms of the incompressible Navier-Stokes equations:

$$\frac{\partial u_i}{\partial x_i} = 0 \tag{2.1}$$

$$\frac{\partial u_i}{\partial t} = -\frac{\partial (u_i u_j)}{\partial x_j} + 2\nu \frac{\partial D_{ij}}{\partial x_j} - \frac{1}{\rho}\left(\frac{\partial p}{\partial x_i} - s_i\right) = -\frac{\partial (u_i u_j)}{\partial x_j} + \nu \frac{\partial^2 u_i}{\partial x_j^2} - \frac{1}{\rho}\left(\frac{\partial p}{\partial x_i} - s_i\right) \tag{2.2}$$

Non-dimensionalization parameters and others:

$$t^* = \frac{tU}{L} \qquad x_i^* = \frac{x_i}{L} \qquad p^* = \frac{p}{\rho U^2} \qquad u^* = \frac{u}{U} \qquad \frac{1}{Fr} = \frac{gL}{u^2}$$

$$P = p^* + \frac{x_2^*}{Fr^2} \qquad s = \begin{bmatrix} 0 \\ -\rho g \end{bmatrix} \qquad 2\frac{\partial D_{ij}}{\partial x_j} = \frac{\partial^2 u_i}{\partial x_j \partial x_j}$$

Mass conservation is non-dimensionalized:

$$\frac{U}{L}\frac{\partial u_i^*}{\partial x_i^*} = 0 \tag{2.3}$$

$$\rightarrow \frac{\partial u_i^*}{\partial x_i^*} = 0 \tag{2.4}$$

The momentum equation is non-dimensionalized:

$$\frac{U^2}{L}\frac{\partial u_i^*}{\partial t^*} = -\frac{U^2}{L}\frac{\partial (u_i^* u_j^*)}{\partial x_j^*} + \frac{\nu U}{L^2}\frac{\partial^2 u_i^*}{\partial x_j^{2*}} - \frac{1}{\rho}\left(\frac{\rho U^2}{L}\frac{\partial p^*}{\partial x_i^*} - \begin{bmatrix} 0 \\ -\rho g \end{bmatrix}\right) \tag{2.5}$$

$$\rightarrow \frac{\partial u_i^*}{\partial t^*} = -\frac{\partial (u_i^* u_j^*)}{\partial x_j^*} + \frac{1}{Re}\frac{\partial^2 u_i^*}{\partial x_j^{2*}} - \frac{\partial p^*}{\partial x_i^*} + \frac{L}{\rho U^2}\begin{bmatrix} 0 \\ -\rho g \end{bmatrix} \tag{2.6}$$

$$\rightarrow \frac{\partial u_i^*}{\partial t^*} = -\frac{\partial (u_i^* u_j^*)}{\partial x_j^*} + \frac{1}{Re}\frac{\partial^2 u_i^*}{\partial x_j^{2*}} - \frac{\partial p^*}{\partial x_i^*} - \begin{bmatrix} 0 \\ \frac{gL}{u^2} \end{bmatrix} \tag{2.7}$$

$$\rightarrow \frac{\partial u_i^*}{\partial t^*} = -\frac{\partial (u_i^* u_j^*)}{\partial x_j^*} + \frac{1}{Re}\frac{\partial^2 u_i^*}{\partial x_j^{2*}} - \frac{\partial P}{\partial x_i^*} \tag{2.8}$$

$$\rightarrow \frac{\partial u_i^*}{\partial t^*} = H_i - \frac{\partial P}{\partial x_i^*} \tag{2.9}$$

In order to derive the pressure equation in 2D, divergence of the non-dimensionalized momentum equation is taken and continuity is invoked, i.e. $\frac{\partial u_i}{\partial t} = 0$:

$$\nabla \cdot \left( \frac{\partial u_i}{\partial t} - H_i + \frac{\partial P}{\partial x_i} \right) = 0 \tag{2.10}$$

$$\rightarrow \frac{\partial}{\partial x} \left( \frac{\partial u}{\partial t} - H_1 + \frac{\partial P}{\partial x} \right) + \frac{\partial}{\partial y} \left( \frac{\partial v}{\partial t} - H_2 + \frac{\partial P}{\partial y} \right) = 0 \tag{2.11}$$

$$\rightarrow \frac{\partial^2 P}{\partial x^2} + \frac{\partial^2 P}{\partial y^2} = \frac{\partial H_1}{\partial x} + \frac{\partial H_2}{\partial y} \tag{2.12}$$

Where

$$H_i = -\frac{\partial (u_i u_j)}{\partial x_j} + \frac{1}{Re} \frac{\partial^2 u_i}{\partial x_j^2} \tag{2.13}$$

# 3 Computation and convergence of discrete H

The $H_1$ and the $H_2$ functions for the Navier-Stokes equations in 2D are computed.
Firstly the boundary conditions for the pressure are found by investigating the vector product of the normal vector to the wall and the momentum equations. For this simple cavity flow it means that on the vertical wall only the x-momentum equation is used and on the vertical wall only the y-momentum equation is used. As the velocities are constant along the boundaries both momentum equations prescribes a homogeneous Neumann boundary condition on the walls.
The $H_1$ function describes the horizontal x-momentum equation and is hence not computed at the north and south walls. The $H_2$ function describes the vertical y-momentum equation and is hence not computed at the east and west walls.
All terms of the H functions can be described with derivatives of the velocity fields:

$$H_1 = \frac{\partial}{\partial x} \left( \frac{1}{Re} \frac{\partial u}{\partial x} - u^2 \right) + \frac{\partial}{\partial y} \left( \frac{1}{Re} \frac{\partial u}{\partial y} - uv \right) \tag{3.14}$$

$$H_2 = \frac{\partial}{\partial x} \left( \frac{1}{Re} \frac{\partial v}{\partial x} - uv \right) + \frac{\partial}{\partial y} \left( \frac{1}{Re} \frac{\partial v}{\partial y} - v^2 \right) \tag{3.15}$$

Thus making it easier to compare with an exact function and validating the functions. The following exact functions are used:

$$u(x, y) = sin(k_1 x) sin(k_2 y) \tag{3.16}$$

$$v(x, y) = sin(k_3 x) sin(k_4 y) \tag{3.17}$$

The difference between the computed functions and the exact functions are showed in figure 3.1 for increasing resolution.

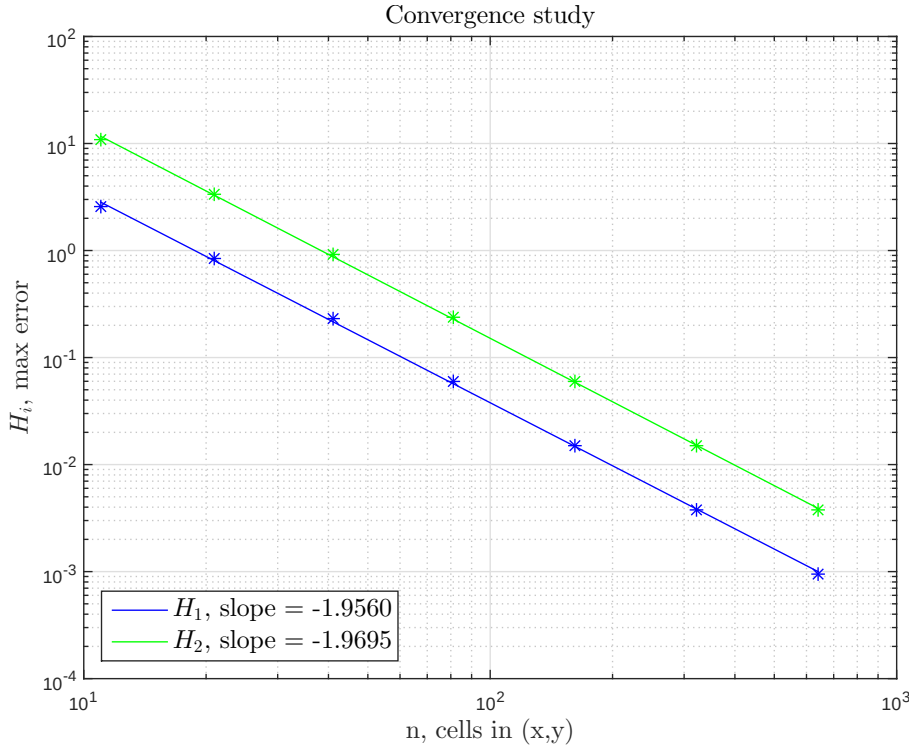


**Figure 3.1:** Convergence study of the error between the exact functions and the $H_1$ and the $H_2$ functions

As expected a second order convergence is obtained for the H functions for increasingly fine resolution, because of the implemented CDS scheme.
In figure 3.2 the H functions are plotted along with the exact functions described above for validation. The computed functions are corresponding well with the exact functions hence validating the computed H functions.

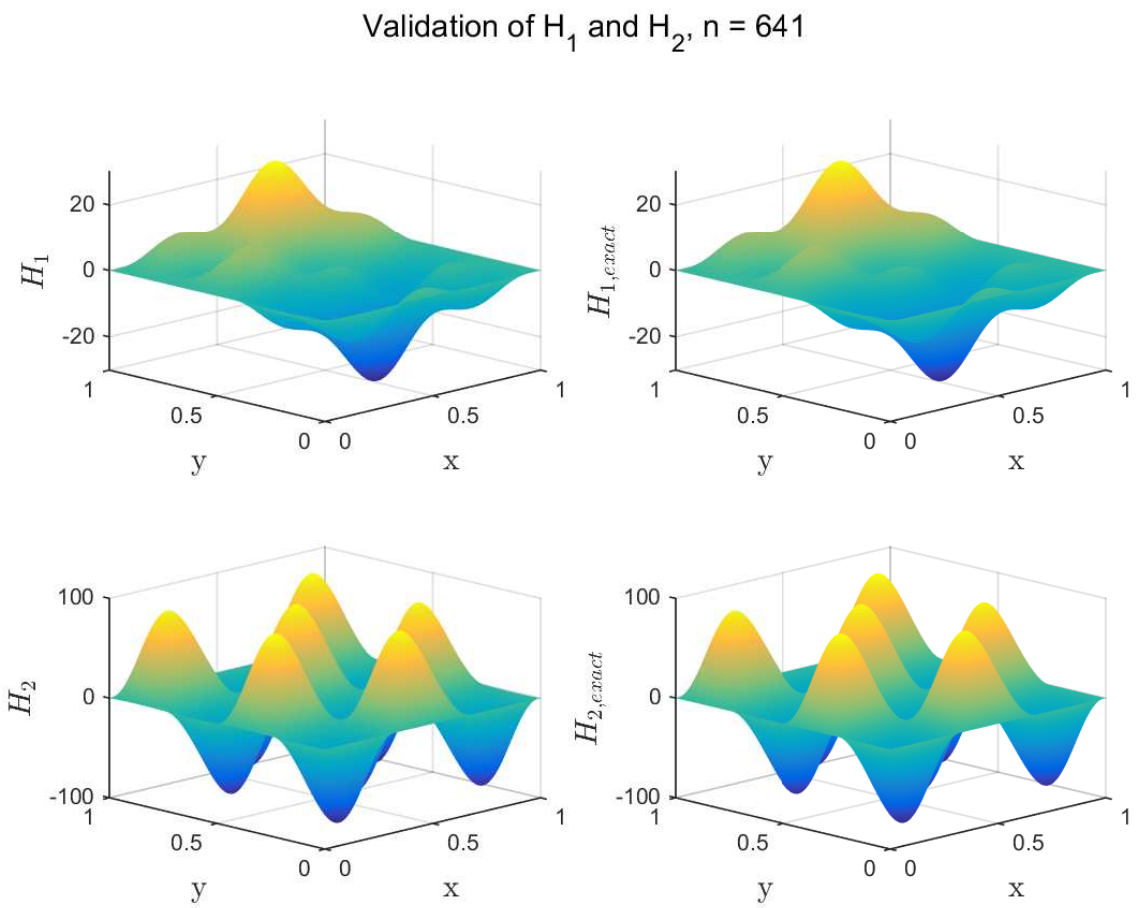


**Figure 3.2:** Computed H functions to the left and exact H functions to the right

# 4 Solving the Poisson equation

After the H1 and H2 functions have been found, the matrix equation can be assembled.

$$\mathbf{Ap} = \mathbf{s} \tag{4.18}$$

The problem investigated in this report is pure diffusion with homogeneous Neumann boundary conditions along all boundaries. CDS discretizing is used, and cell wall fluxes can be calculated from page 138[1]. After implementing the boundary condition, the 2D Laplacian operator matrix can be found. The source term is calculated from the discrete **H** functions:

$$\mathbf{s} = \left.\frac{\partial P}{\partial x}\right|_w^e \Delta y + \left.\frac{\partial P}{\partial y}\right|_s^n \Delta x = H_1|_w^e \, \Delta y + H_2|_s^n \, \Delta x \tag{4.19}$$

No correction to the source term is needed due to $H_1$ being zero on vertical walls and $H_2$ being zero on horizontal walls as described in section 3. Due to no Dirichlet boundary condition is enforced,the rank of A becomes $n^2 - 1$ and the system is singular. Therefore an infinite number of solutions exist. This means that the resulting pressure matrix have to be calibrated to a

known value to avoid fluctuations (i.e. Dirchlet condition). For our cavity flow, the center value of the pressure is set to zero.

**P-test function:**
To validate the pressure solution, the following test functions are used:

$$H_1 = -k \cdot sin(kx)cos(ky)$$
$$H_2 = -k \cdot cos(kx)sin(ky)$$
$$P_{exact} = cos(kx)cos(ky)$$

Using these test functions, a convergence study has been performed in order to validate the solver.

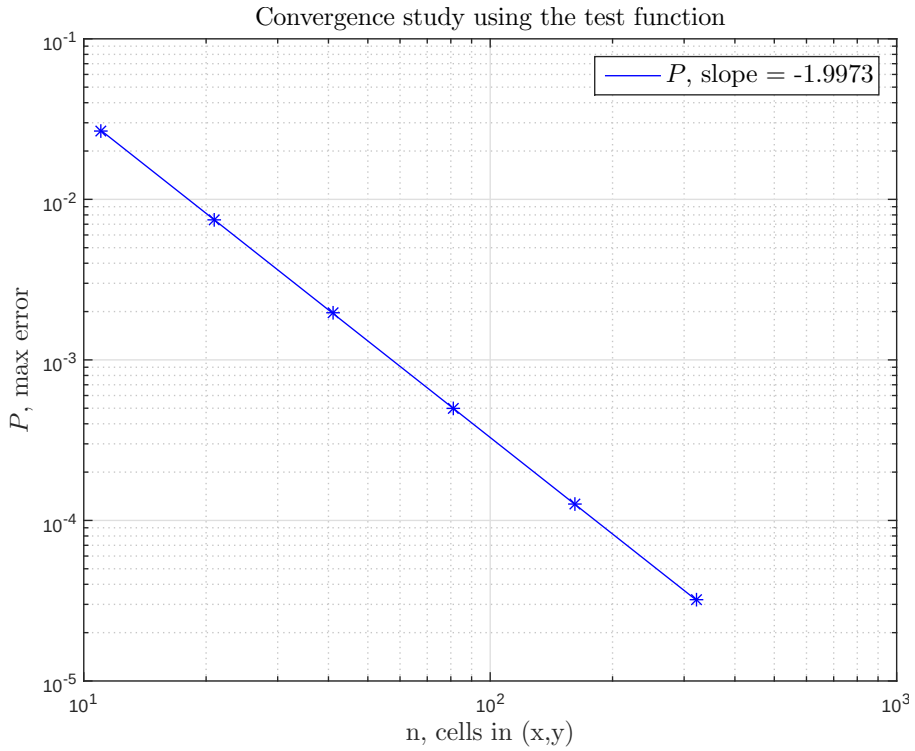


**Figure 4.3:** Convergence study of the pressure solver using the test function

It can be seen from figure 4.3 that the solution converges with second order accuracy, which was expected due to the implemented second order CDS scheme. The used test functions and the pressure have been visualized in figure 4.4 for N=321. Here it can be noted that the error is zero at the center values due to the recalibration of the singular system.

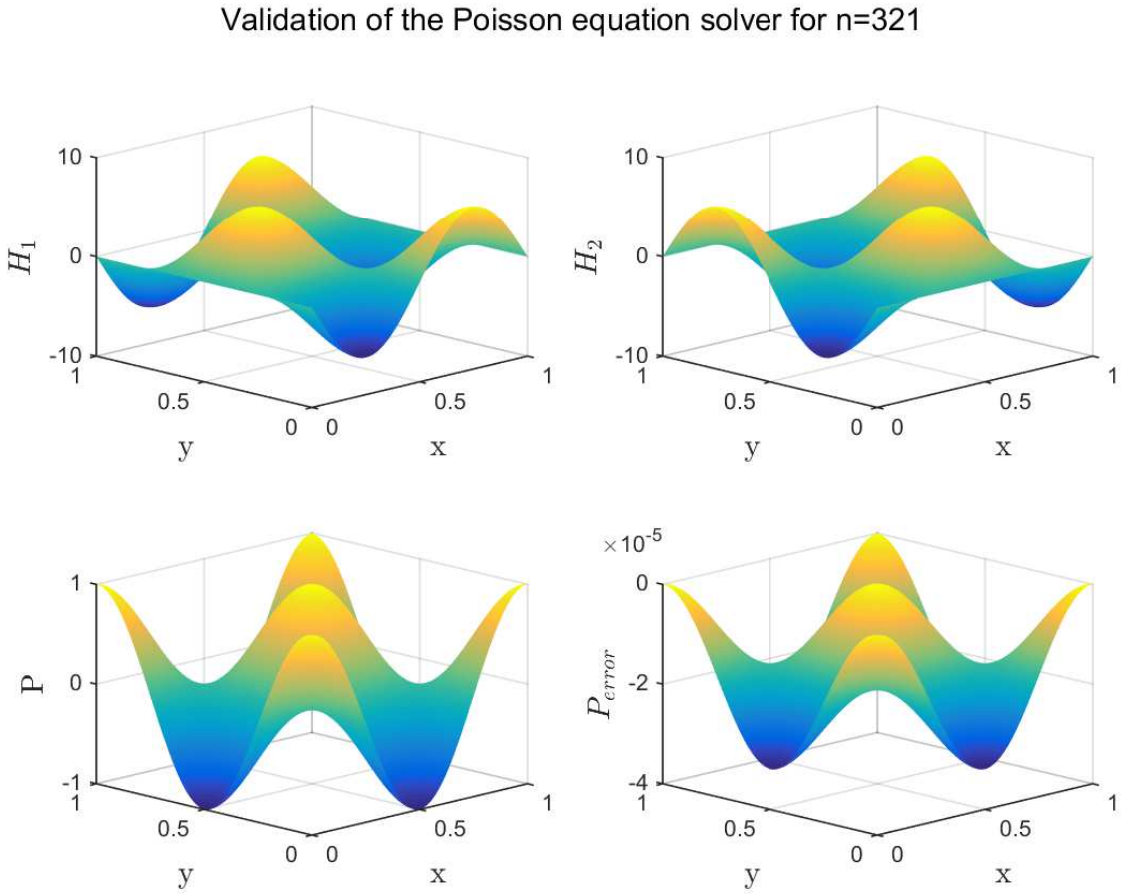


**Figure 4.4:** Visualization of the used H functions, the found pressure and the error at N=321

# 5 Implementation of the explicit Euler time stepping method

After computing the functions $H_1$ and $H_2$ and solving the pressure the Explicit Euler time stepping method is used to find the velocity field at time step m+1:

$$u_{m+1} = u_m + \Delta t \left( H_1 - \frac{\partial P}{\partial x} \right)_m \tag{5.20}$$

$$v_{m+1} = v_m + \Delta t \left( H_2 - \frac{\partial P}{\partial y} \right)_m \tag{5.21}$$

To use this method one has to consider the stability of the system hence deciding the size of the time step used. For $Re << 1$ the convective terms are ignored and the stability limit only depends on the viscosity(diffusion). At high Reynolds numbers the viscous terms can be ignored and the stability limit is described by a linearized convection. This yields an approximate stability criteria that covers a broad range of Reynolds numbers:

$$\Delta t \leq min \left( \frac{Re \Delta x^2}{4}, \frac{1}{U^2 Re} \right) \tag{5.22}$$

The velocity scale is set to the lid velocity, U=1, which is an approximation and not appropriate for all Reynolds numbers. The choice of using lid velocity is also a conservative guess in order to avoid unexpected instability
Due to limited computational resources a steady-state tolerance is introduced. The steady state solution is reached when the maximum change in the velocity field per unit time is less than the steady-state tolerance. The tolerance is selected to be $10^{-5}$ as it fits well with the number of significant figures provided in the benchmark table[2].

# 6 Creeping flow Re=1, n=21

The H functions, pressure solver and time stepping scheme can now be combined to solve the actual cavity flow. The flow is solved for a very low Reynolds number on a coarse grid and a steady state tolerance of $10^{-5}$ is used. This means that steady state is assumed achieved when the maximum velocity change for each time step is less than steady state tolerance value. For the creeping flow, this state is achieved only 0.3 seconds after the flow is initialized. The SST flow is visualized using streamlines and compared qualitatively with the plot provided in the assignment. It can be seen from figure 6.5 that the flow solution is comparable to the provided steady state solution.

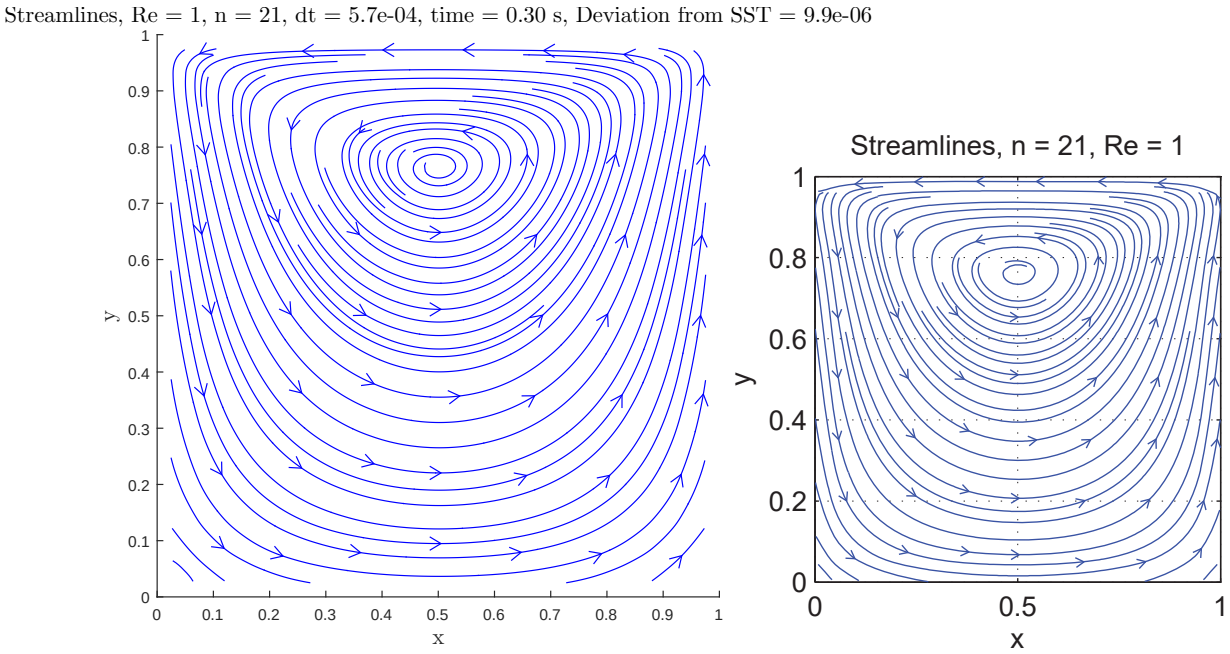


**Figure 6.5:** Solutions for Re=1, n=21. Left: Solver result Right: Provided solution for same condition

The deviation from steady state over time and the pressure field is plotted in figure 6.6. It can be noted from the pressure plot that two singularities exist in the flow, one at the top left stagnation point and one at the top right flow singularity. From the deviation from steady state plot, it can be noted that the solution achieves steady state very fast, which is expected for a creeping flow.

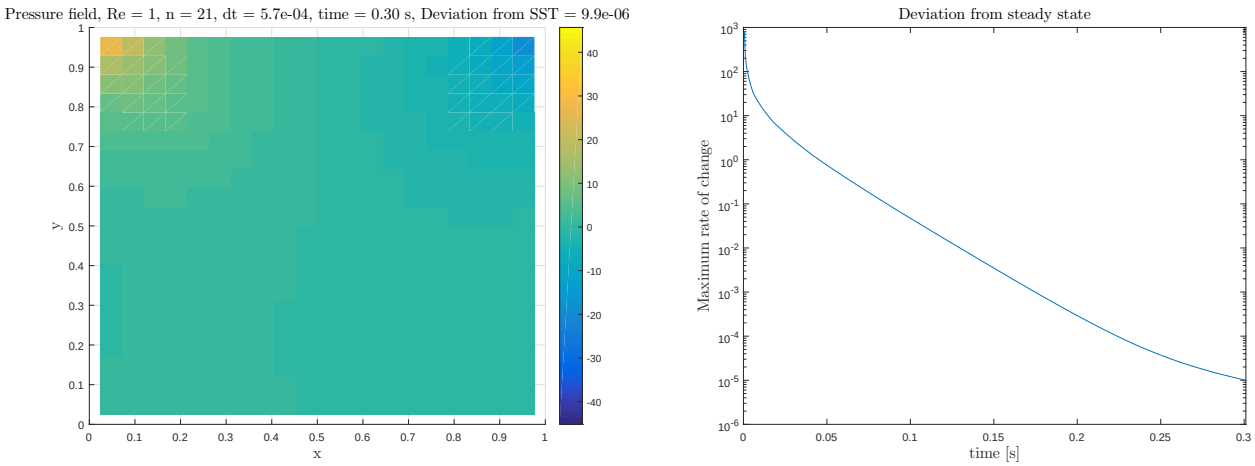


**Figure 6.6:** Left: Pressure plot of the solution Right: Deviation from the steady-state solution

The left side of figure 6.7 shows the local continuity errors. This figure shows a linear increasing trend with the number of time steps. For this specific problem the error is small($10^{-14}$) and close to machine precision. However for problems with different Reynolds number and grid size the error could become significant over time. This problem is dealt with in section 7. The plot to the right in figure 6.7 shows that global conservation of mass is fulfilled to machine precision, which also is a necessity for this to be a valid solution.

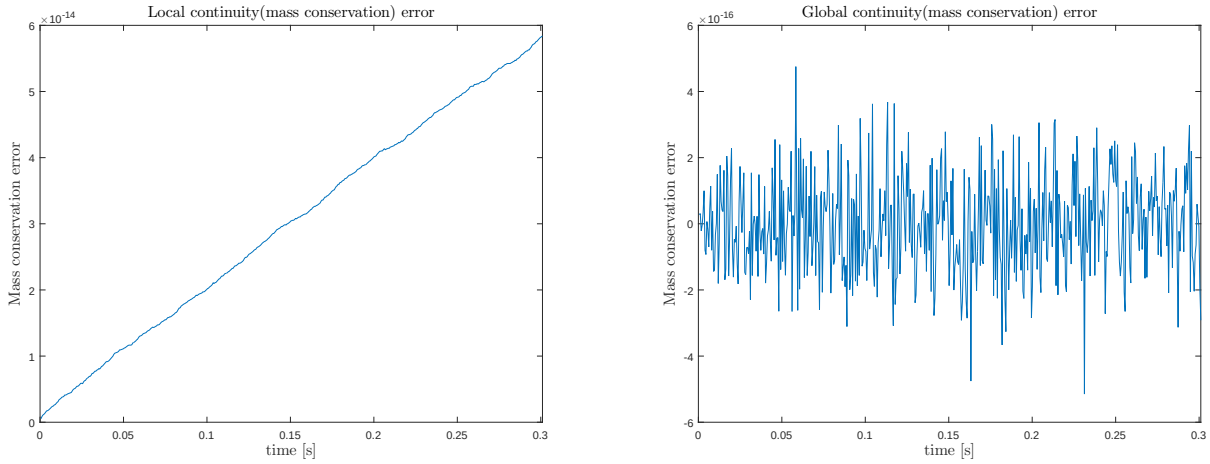


**Figure 6.7:** Left: Local continuity error Right: Global continuity error

# 7 Discrete Continuity Correction

When deriving the Poisson equation the old velocity field is assumed divergence free:

$$\cancel{\frac{\partial}{\partial t}(\nabla \cdot u)} = \nabla \cdot H - \nabla^2 P \tag{7.23}$$

This means that local continuity errors grow linearly with time hence there is no local mass-conservation, see the left side of figure 6.7.
At this time the continuity error is small but growing. Hence for longer simulations this will be

a problem. To avoid this problem the pressure must be computed such that the velocity field at the new timestep is divergence free on the discrete level:

$$\nabla^2 P_{m+1} = \nabla H_m + \frac{1}{\Delta t} (\nabla u_m) \tag{7.24}$$

The corrected Poisson problem ensures no accumulation of discrete continuity errors, see figure 7.8.

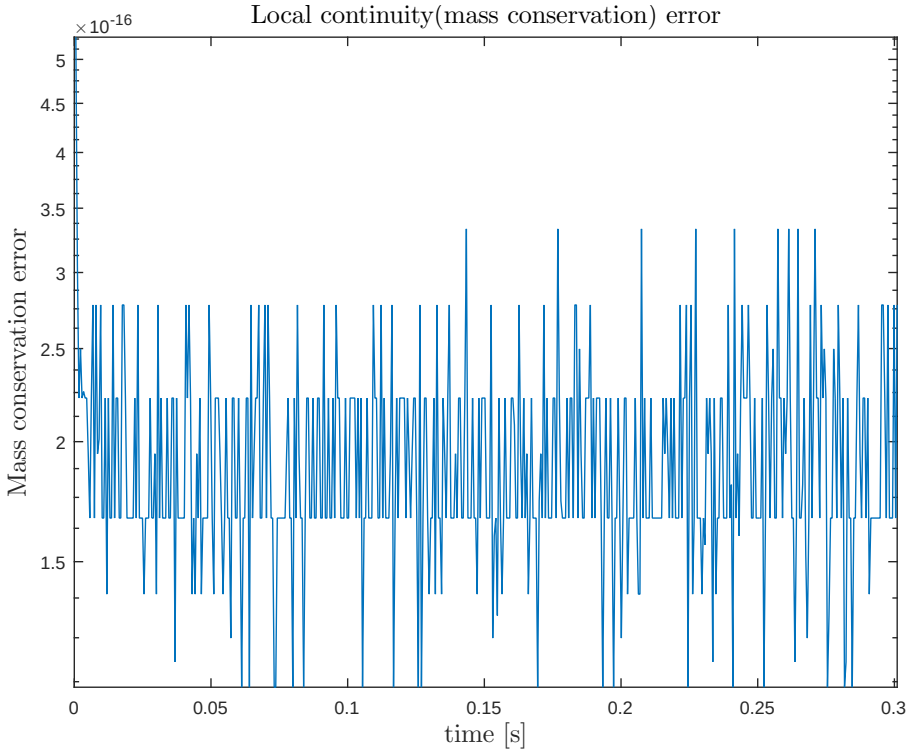


**Figure 7.8:** Local continuity error with the corrected Poisson problem

# 8 Increasing the efficiency of the solver

To increase the efficiency of the solver a reordering and lu-factorizing of the time-constant matrix **A** is carried out before any time-step. For each time step the factorized matrix is used to solve the discrete Poisson equation. Figure 8.9 shows the computational time for different values of n before and after optimizing the solver. The figure clearly shows that the computational time used to solve is dramatically decreased when using the optimized solver.

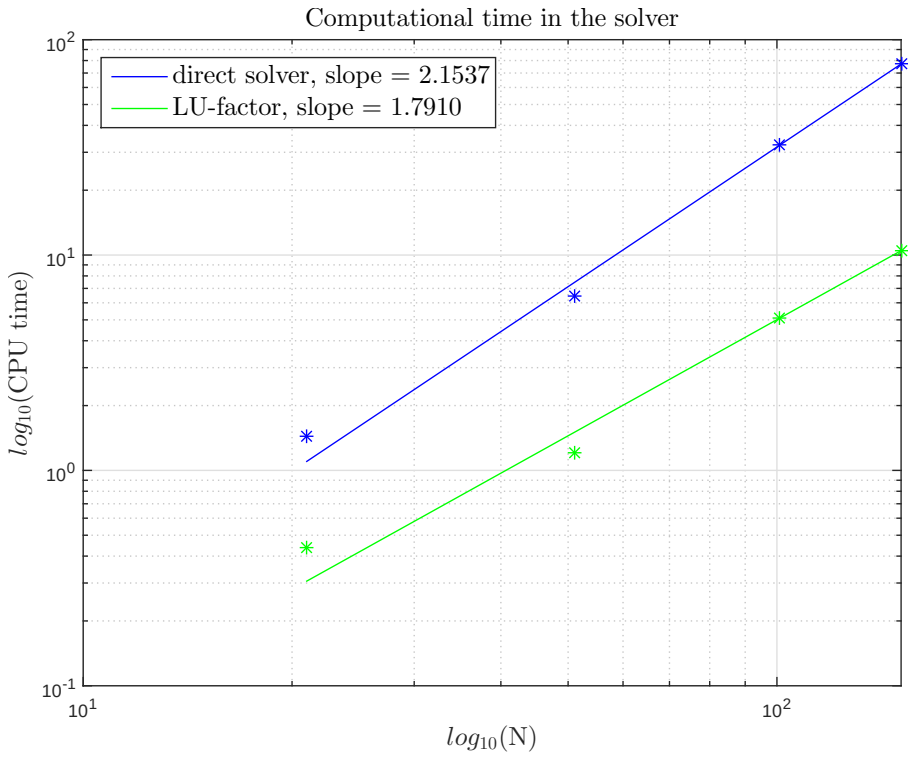


**Figure 8.9:** Computational time for varying number of grid points, n, at Re=1000 and for 1000 timesteps

# 9 Benchmarking

For n=21 and Re=1000 a comparison between the solver and a provided plot is carried out. A steady state tolerance of $10^{-5}$ is used and now it takes almost 100 seconds before the flow reach this definition of a steady state. In figure 9.10, the steady state solution has been compared to provided flow visualization and they seem to fit very well with each other considering the vortex positions and sizes.

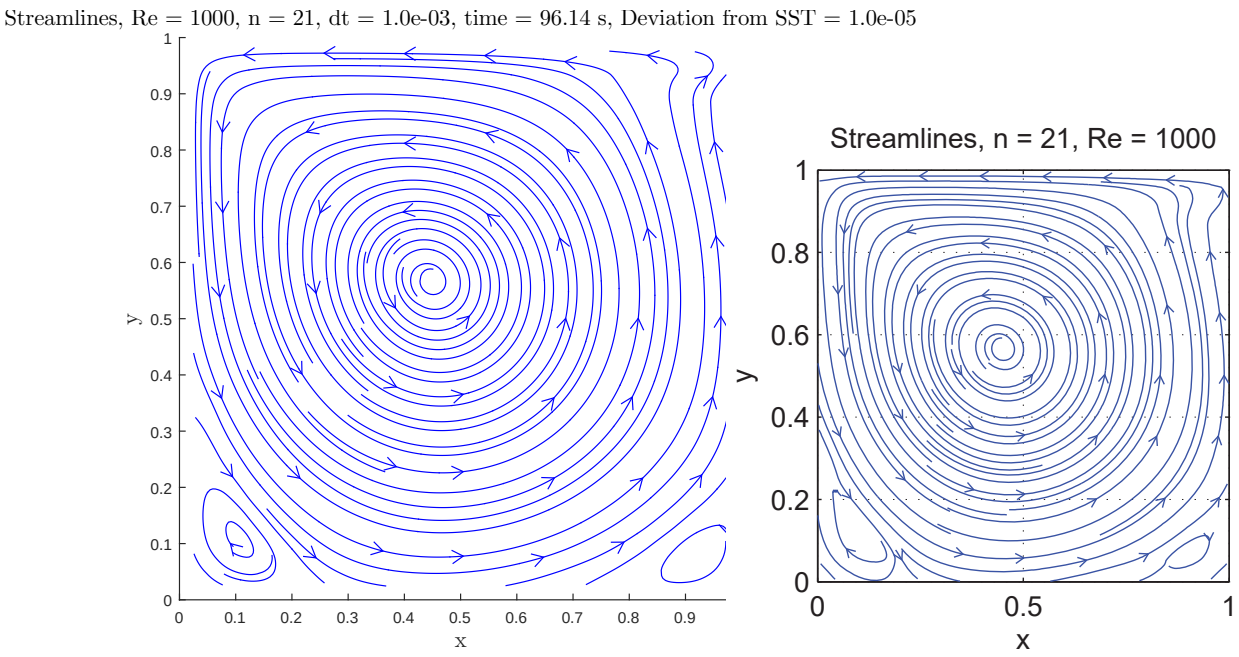


**Figure 9.10:** Solutions for Re=1000, n=21. Left: Solver result Right: Provided solution for same condition

The solution at Re=1000 is then verified for a low resolution. For final confirmation of the solution it is compared to the litterature[2]. This is done for increasing resolution and the results can be seen in figure 9.11.

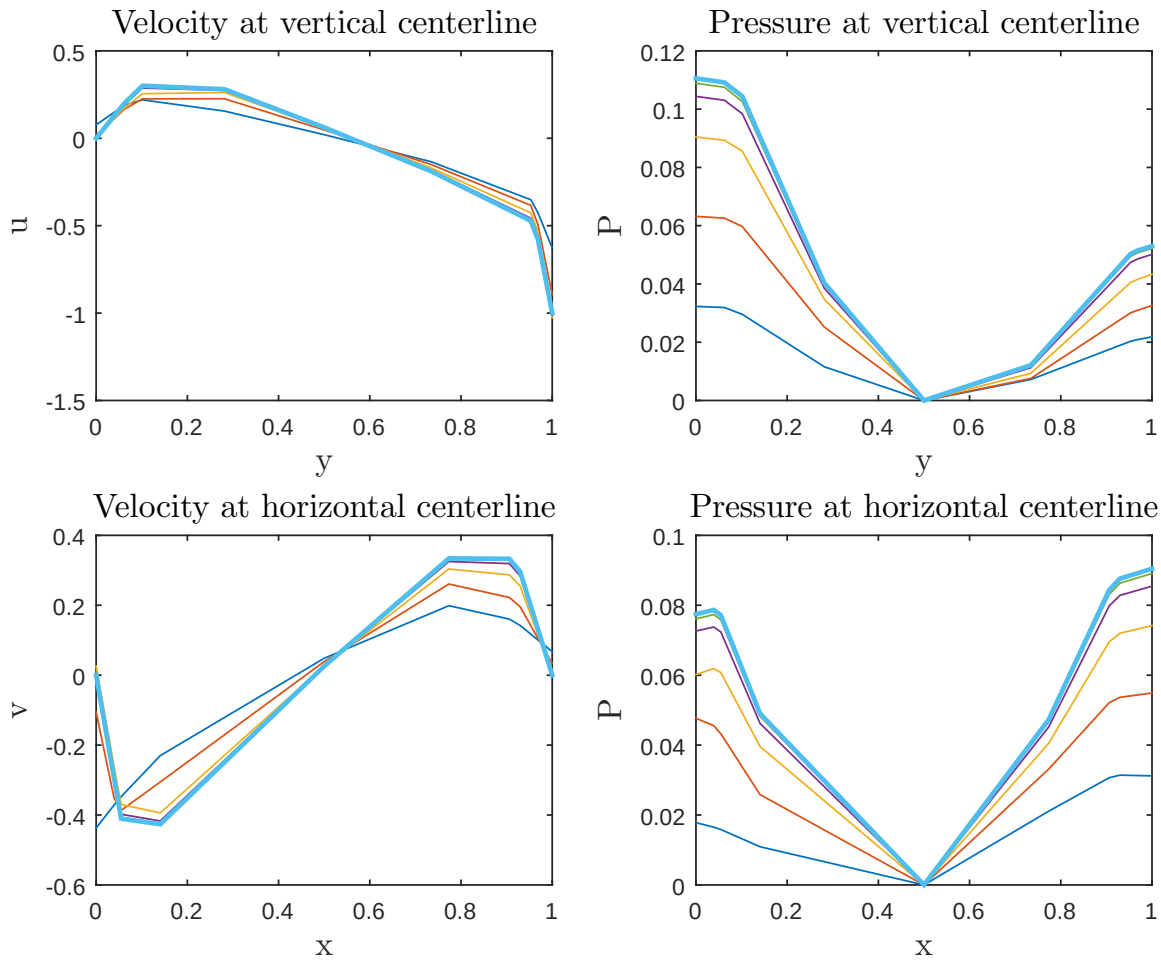


**Figure 9.11:** Bold light blue curve is experimental results[2], green(n=161), purple(n=81), yellow(n=41), orange(n=21) and dark blue(n=11)

At the highest resolution with n=161 the solver overall agrees with the results from the literature. The figure clearly shows a converging trend for increasing resolution.
The maximum error is found at every iteration and the rate of convergence is found for the investigated parameters, see figure 9.12.

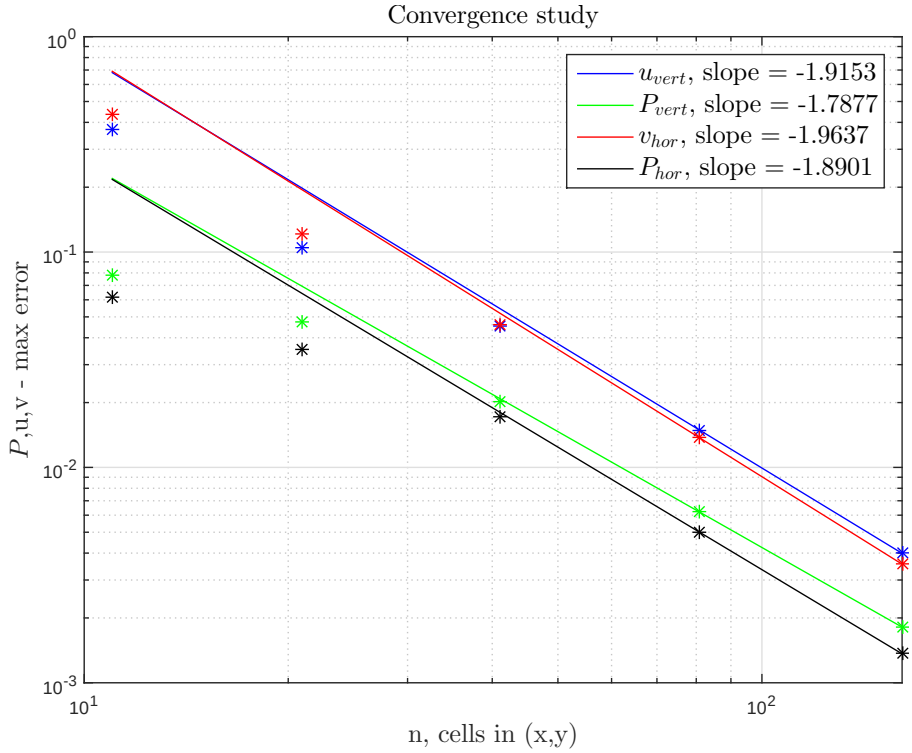


**Figure 9.12:** Rate of convergence for the parameters investigated in the litterature[2]

As expected for a CDS scheme the rate of convergence for the velocities and pressure is close to being second order. If the steady-state tolerance was decreased and more significant digits for the reference flow were given, the slope would probably be closer to 2.
Since figure 9.11 shows a good coherence between the litterature and the solver results for n=161. The following plots are taken at this resolution:

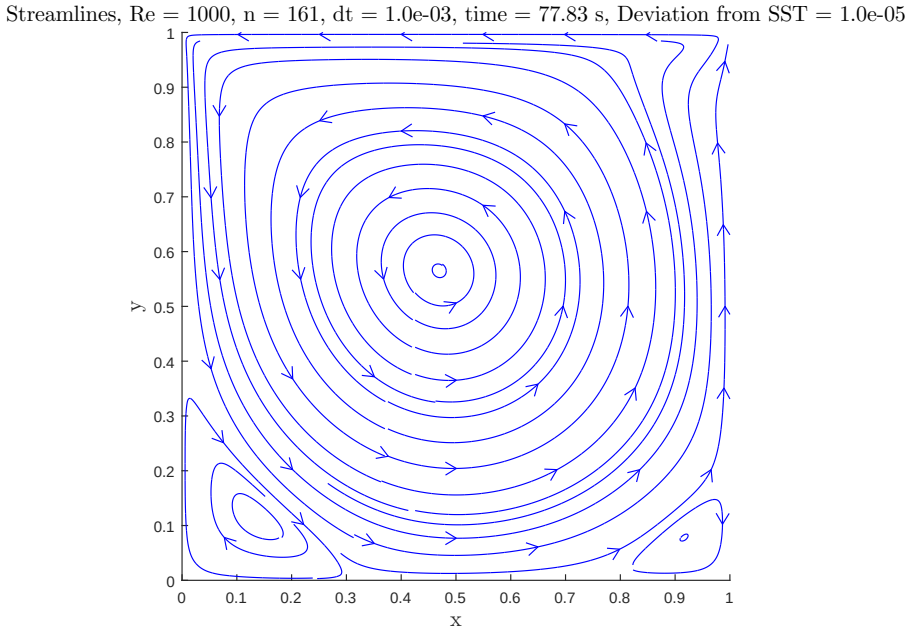


**Figure 9.13:** Streamlines for Re=1000 and n=161

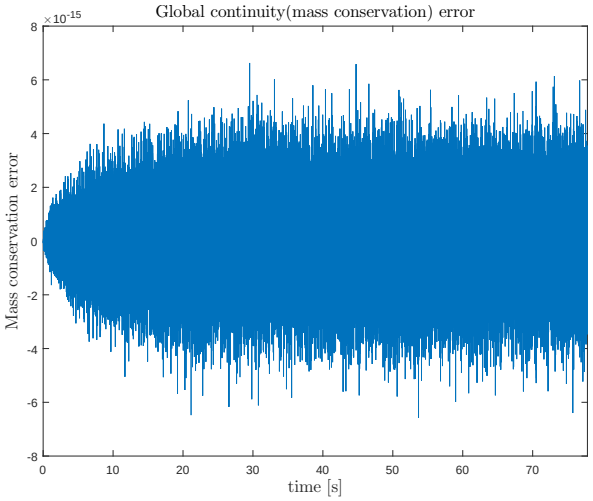


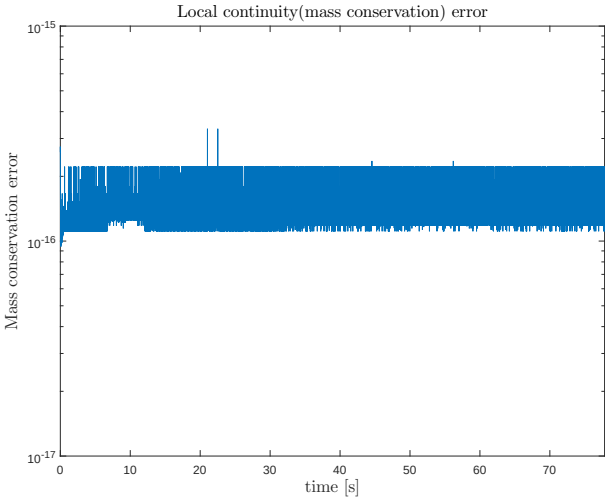


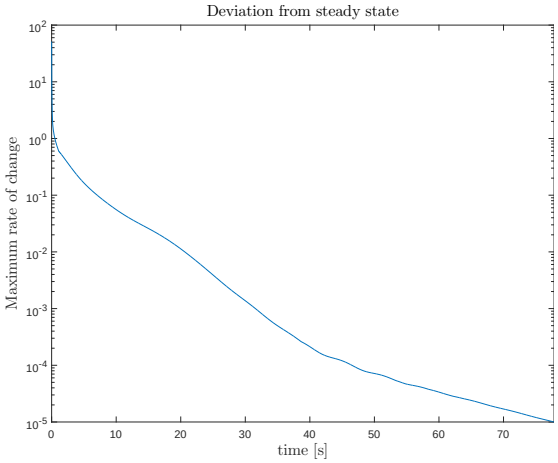


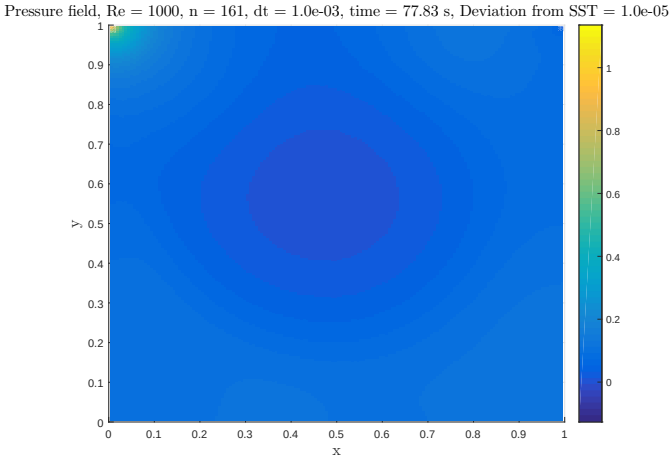


**(a)** The maximum rate of change as function of physical time

**(b)** Pressure plot with stagnation point at top left corner

It should be noted that the main vortex is also visible in the pressure plot along with the two singularities.

# References

[1] Harry B. Bingham, Poul S. Larsen, V. Allan Barker, DTU Mekanik, *"Computational Fluid Dynamics"*, 2015

[2] Bruneau and Saad, 2006